Manipulating optical Tamm state in the terahertz frequency range with graphene

Leyong Jiang (蒋乐勇)[1], Jiao Tang (唐 娇)[1], Qingkai Wang (王庆凯)[2], Yuexiang Wu (吴粤湘)[2], Zhiwei Zheng (郑之伟)[1], Yuanjiang Xiang (项元江)[2], and Xiaoyu Dai (戴小玉)[2,*]

[1]*School of Physics and Electronics, Hunan Normal University, Changsha 410081, China*
[2]*International Collaborative Laboratory of 2D Materials for Optoelectronic Science & Technology of Ministry of Education, College of Optoelectronic Engineering, Shenzhen University, Shenzhen 518060, China*
**Corresponding author: xiaoyudai@126.com*

Received October 26, 2018; accepted December 14, 2018; posted online January 29, 2019

The optical Tamm state (OTS), which exists generally at the interface between metal and a dielectric Bragg mirror, has been studied extensively in the visible and near infrared spectra. Nevertheless, OTS in the terahertz (THz) region normally receives far less attention. In this Letter, we demonstrate the physical mechanism of OTS at the interface between graphene and a dielectric Bragg mirror in the THz frequency band by applying the transfer matrix method and dispersion characteristics. Based on such mechanisms, we propose an efficient method that can precisely generate and control OTS at a desired angle and frequency. Moreover, we show that the OTS is dependent on the optical conductivity of graphene, making the graphene–dielectric-Bragg-mirror a good candidate for dynamic tunable OTS device in the THz frequency range.

OCIS codes: 160.4236, 250.5403.
doi: 10.3788/COL201917.020008.

The optical Tamm state (OTS) is a kind of surface wave confined at the interface between two different media. It is an optical analogue of electronic Tamm state predicted by Tamm and firstly occurs at the boundary between two periodical dielectric structures[1,2]. In the past few years, OTS has attracted particular attention due to its potential applications in polariton laser fabrication and enhanced light–matter interaction, as well as nanolasers, thermophotovoltaic devices[3–6], etc. Very recently, a unidirectional all-OTS-based absorption switch has also been reported[7]. In comparison with the conventional surface waves [e.g., surface plasmon polaritons (SPPs)], OTS can be excited directly for both the TE- and TM-polarized waves and occur even at normal incidence[8]. Therefore, OTS represents an excellent alternative for a variety of optical elements with a functionality relying on surface waves. Researchers have been intrigued by the possibility of using different methods for realizing OTS through various materials and configuration systems, such as one-dimensional (1D) magnetophotonic structures[9–11], two-dimensional (2D) materials[12,13], photonic crystal (PC) heterostructures[14–16], metal–Bragg-reflector structures[17,18], and plasmonic waveguides[7,19]. It is well known that the ability to create and manipulate OTS in a terahertz (THz) frequency range is central to the development of micro/nano optical components. It has been reported that OTS can be controlled by an external magnetic field[20], anisotropic materials[21], etc. However, there are very few reports concerning tunable OTS, especially in the THz frequency range.

Recently, graphene, a one-atom-thick 2D carbon material, has attracted intensive interest due to its unique optical and electrical properties[22–29]. Graphene in a micro/nano structure is extremely promising for various optoelectronic applications, including a graphene-based broadband polarizer[30], fiber laser[31], metamaterials[32–36], etc. Besides, graphene is a zero bandgap material, and its electromagnetic response can be realized from the ultraviolet to THz range[37]. Therefore, graphene-based optoelectronic devices could work over a much broader wavelength range. Apart from being a special bandgap structure, graphene is also attractive for the possibility of controlling its carrier concentration via external gate voltages or chemical doping. It means graphene's conductivity can be continuously tuned in a broad frequency range by shifting the Fermi energy. In addition, graphene is intrinsically a semimetal with some metallic properties under certain conditions[38–40]. Interesting questions arise as to whether graphene can be used to realize OTS in a PC structure or, more importantly, whether such a graphene–PC composite structure could support the controllable OTS. To answer these questions, in this Letter, we investigate theoretically the tunable OTS of a graphene–PC structure in the THz frequency range using the modified transfer matrix method[41]. It is found that the OTS in this composite structure can be realized due to electric field enhancement and the giant linear conductivity of graphene. Furthermore, we have confirmed a way to manipulate OTS by tuning the Fermi energy of graphene, adjusting the incident angle, and varying the thickness and permittivity of the top layer. Graphene-based controllable optical devices with intrinsic OTS allow us to find potential applications in optical absorption, optical sensing, and some other optoelectronics fields.

It is known that 1D PC heterostructures and distributed Bragg reflector (DBR) structures are the two most ideal structures for observing OTS phenomena. Here, we consider a composite structure composed of graphene and a 1D PC. A top layer is placed between graphene and a 1D PC, where d_s is the thickness of the top layer adjacent to graphene, as presented in Fig. 1. This configuration can be seen as an asymmetrical cavity consisting of a graphene layer on the left side and a DBR on the right side; the top layer is located inside the cavity. The 1D PC is made of 20 pairs of alternate dielectric layer 1 (with refractive index n_1 and thickness d_1) and dielectric layer 2 (with refractive index n_2 and thickness d_2). We focus on an experimentally relevant structure in the THz region and assume that dielectric 1 is polymethylpentene (TPX) with $n_1 = 1.46$ and dielectric 2 is SiO_2 with $n_2 = 1.9$[42]. TPX is a transparent material in both visible light and the THz frequency range (0.6–6 THz).

Above the top layer is the graphene sheet. Within the local random phase approximation and without considering the external field, the surface conductivity of the graphene sheet is dominated by the intraband term in the THz range, namely,

$$\sigma(\omega) \approx \frac{ie^2 k_B T_g}{\pi\hbar^2(\omega + i/\tau)}\left[\frac{E_F}{k_B T_g} + 2\ln\left(e^{-\frac{E_F}{k_B T_g}} + 1\right)\right], \quad (1)$$

where E_F is the Fermi energy, ω is the frequency of the incident light, τ is the electron–phonon relaxation time, and T_g is the temperature in Kelvin. e, k_B, and $\hbar$ are the universal constants related to the electron charge, Boltzmann constant, and reduced Planck's constant, respectively. Here, the Fermi energy E_F can be electrically controlled by an applied gate voltage, thereby leading to a tunable surface conductivity. This could provide an effective route to achieving controlled transmission and reflection characteristics in graphene–1D-PC composite structure. Besides, we choose the center wavelength of $\lambda_c = 300$ μm, $E_F = 0.75$ eV, $\tau = 1$ ps, and $T_g = 300$ K for graphene. The other parameters are taken as $d_j = \lambda_c/4n_j$ and $j = 1, 2$. For simplicity, we assume the refractive index n_s and the thickness d_s of the top layer are the same as those of dielectric layer 2.

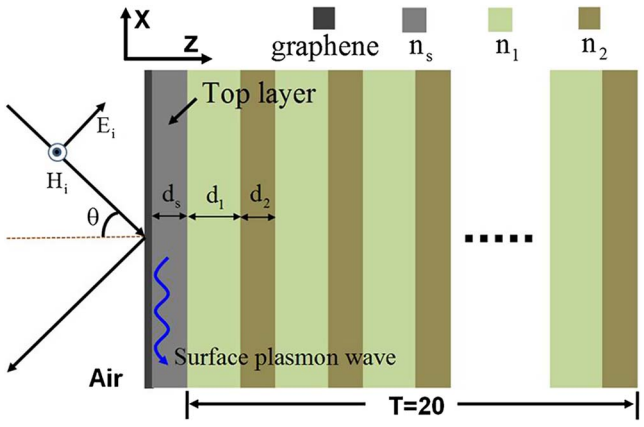

Fig. 1. Schematic diagram of the graphene–1D-PC composite structure. Incident light is assumed to be TM-polarized. Surface of the graphene layer is defined as the plane of $z = 0$. Here, the period for the PC is $T = 20$.

To obtain the resonance condition associated with OTS, we use the modified transfer matrix method to calculate the transmission and reflection coefficients[41]. Unlike the transmission matrix at the interface of common materials, the transmission matrix at the interface of the air–graphene top layer can be modified as

$$D_{\text{vt}} = \frac{1}{2}\begin{bmatrix} 1+\eta_p+\xi_p & 1-\eta_p-\xi_p \\ 1-\eta_p+\xi_p & 1+\eta_p-\xi_p \end{bmatrix}, \quad (2)$$

where, for the TM-polarized, $\eta_p = \varepsilon_a k_{sz}/\varepsilon_s k_{az}$, $\xi_{\text{p}} = \sigma k_{sz}/\varepsilon_0\varepsilon_s\omega$, $k_{az} = (\omega/c)\cos\theta$, $k_{sz} = k_0\sqrt{\varepsilon_s - \varepsilon_a \sin^2\theta}$, and θ and ε_0 are the incident angle of incident light and the permittivity in the vacuum, respectively. ε_a and ε_s are the dielectric constant of air and the top layer, respectively. Similarly, by applying the boundary conditions and Ohm's law, the transmission matrix for the TE-polarized can be modified as

$$D_{\text{at}} = \frac{1}{2}\begin{bmatrix} 1+\eta_s+\xi_s & 1-\eta_s+\xi_s \\ 1-\eta_s-\xi_s & 1+\eta_s-\xi_s \end{bmatrix}, \quad (3)$$

with the parameters $\eta_s = k_{sz}/k_{az}$ and $\xi_s = \sigma\mu_0\omega/k_{az}$, where μ_0 is the permeability in the vacuum. According to Eqs. (2) and (3), σ can be reflected in the boundary conditions. Hence, we can ignore the thickness of graphene in the computation. Based on the transfer matrix, we can easily calculate the reflectance and the transmittance of the graphene–1D-PC composite configuration.

Now, we discuss the OTS in the graphene–1D-PC composite configuration. It is well known that OTS can be directly excited in both the TE- and TM-polarized waves and could occur even at normal incidence. To simplify the discussion, in the present Letter, we mainly discuss the OTS for TM polarization. In the absence of the graphene layer, and hence lacking OTS in the graphene–1D-PC composite configuration, there is only a photonic bandgap between 275 μm and 330 μm. In Fig. 2, we show the reflectance for the PC with $T = 20$. Due to the neglect of the loss in dielectrics, the reflectance would reach the peak (100%), as shown in Fig. 2(a). However, when the single-layer graphene covers the top layer, the OTS would be appearing as a sharp dip at 315 μm. There is an obvious reflectance dip in the bandgap region. This reflectance dip is deep and relatively narrow due to the long wavelength region, and it is excited by OTS at the interface of the air–graphene top layer. In this novel OTS, the graphene is similar to a mirror surface due to its analogous properties with metal. The electric field confinement in graphene is achieved as a result of its positive imaginary optical conductivity (the effective permittivity is negative). The field confinement in the periodical structure is caused by the

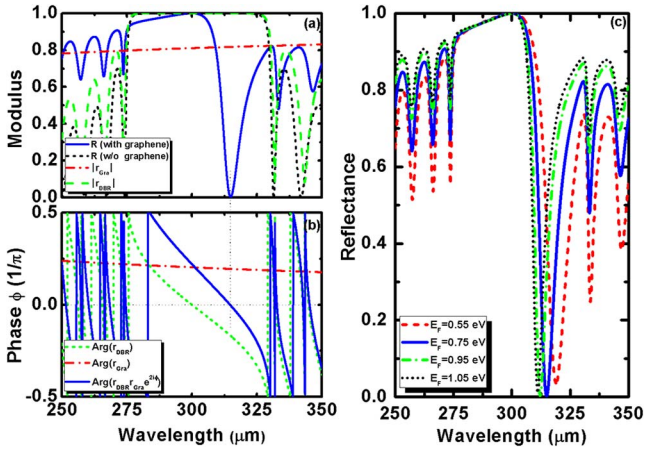

Fig. 2. (a) Reflectance of the graphene–1D-PC configuration (solid line), reflection coefficient r_{Gra} for a graphene top-layer interface (dash dot line), and reflection coefficient r_{DBR} for a top-layer PC interface (dash line) as functions of wavelength. For comparison, the reflectance of the configuration without the graphene layer is also shown (short dash line). (b) The phases of r_{Gra} (dash dot line), r_{DBR} (short dash line), and $r_{\mathrm{DBR}} r_{\mathrm{Gra}} e^{2i\phi}$ (solid line) as functions of wavelength. (c) The reflectance as a function of wavelength for different Fermi energies in the graphene–1D-PC composite configuration.

photonic bandgap of the PC. The OTS occurs owing to the coupling of the electric field in graphene and the PC. The excitation condition of the OTS can be expressed by a formula, namely, $r_{\mathrm{Gra}} r_{\mathrm{DBR}} \exp(2i\phi) = 1$, where r_{Gra} is the reflection coefficient for the electromagnetic wave incident on the graphene layer from the top layer, r_{DBR} is the reflection coefficient of the electromagnetic wave incident on the 1D PC from the same top layer, and ϕ is the phase change of the electromagnetic wave propagating in the cavity between the two interfaces. The above expression can help us estimate the location of the resonance frequency for exciting the OTS. In the calculation of Figs. 2(a) and 2(b), we also use the modified transfer matrix method to obtain $r_{\mathrm{DBR}} = -0.86 + 0.5i$ and $r_{\mathrm{Gra}} = 2/(1+\eta+\xi) - 1$ around 315 μm, where $\eta = \varepsilon_s k_{az}/\varepsilon_a k_{sz} = 1.9$ and $\xi = \sigma k_{az}/\varepsilon_0 \varepsilon_a \omega$. For $\sigma = 0$ (without the graphene layer), $|r_{\mathrm{Gra}}| \ll 1$ and the OTS cannot be excited in this case. However, the introduction of the conductivity of graphene allows large ξ and thus satisfies $r_{\mathrm{Gra}} r_{\mathrm{DBR}} \cdot \exp(2i\phi) \approx 1$. Moreover, the above excitation condition also requires $\mathrm{Arg}[r_{\mathrm{Gra}} r_{\mathrm{DBR}} \exp(2i\phi)] = 0$, and we also obtain $\mathrm{Arg}[r_{\mathrm{Gra}} r_{\mathrm{DBR}} \exp(2i\phi)] \approx 0$ around 315 μm, as shown in Fig. 2(b). This zero-crossing coincides with the reflectance dip in Fig. 2(a). In addition, we further find that the transmittance can almost decrease to 0 with the presence of the graphene sheet, and the absorption has reached almost 100% (not shown in the figure). It is clear that this wavelength-dependent absorption can be used to design wavelength absorbers in the THz range.

Another advantageous and interesting feature of the graphene–1D-PC composite configuration is the tunable wavelength-selected range achieved by changing the Fermi energy E_F. The electrically tunable Fermi energy provides us with a method for manipulating the reflectance, as shown in Fig. 2(c). The reflectance dip of the composite configuration first decreases and then increases with increasing Fermi energy E_F. At the same time, the reflectance dip moves to the shorter wavelength side when we increase the Fermi energy E_F. For $E_F = 0.55$ eV, the wavelength of the reflectance dip is $\lambda = 319$ μm; however, for $E_F = 1.05$ eV, the wavelength of the reflectance dip is $\lambda = 311$ μm. This property suggests that the wavelength of the reflectance dip can be manipulated by the Fermi energy of the graphene layer. It is quite useful, and we can realize the manipulation of transmission and reflection properties easily by tuning the Fermi energy. It enables us to use the graphene–1D-PC composite configuration in tunable wavelength filtering or absorption in a fixed structure.

To better illustrate the OTS excited by graphene, we perform the simulation using the transfer matrix method and show the electric field distribution along the z axis in the graphene–1D-PC composite configuration at $\lambda = 315$ μm, as shown in Fig. 3. For the sake of better comparison, we have also presented the electric field distribution in a graphene-free 1D PC composite configuration, as shown in Fig. 3(a). The calculated electric field is normalized by the incident electric field, and we set the position of graphene to be $z = 0$. It is found that the electric field decays rapidly for $z > 0$. However, the situation can be obviously changed by introducing monolayer graphene. It is obvious that the electric field is strongly enhanced in the graphene–1D-PC composite configuration, and a maximum electric field can be observed near the boundary between the air and the top layer. The electric field near the interface between the air and top layer has increased to about 30 times larger than that in Fig. 3(a) (in arbitrary

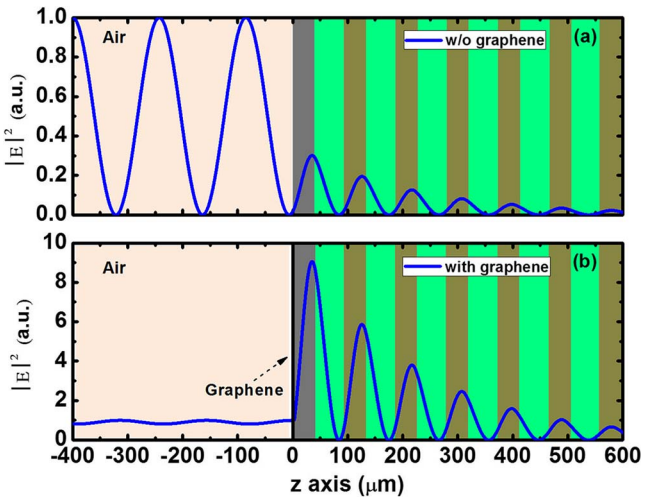

Fig. 3. (a) Normalized electric field profile distributions in the multilayer configuration without the covering of a single graphene layer. (b) Normalized electric field profile distributions in the multilayer configuration with the covering of a single graphene layer.

units). Most of the energy of the electric field is concentrated near the interface between the air and the top layer. At the same time, as the propagating distance in the composite configuration increases, the electric field decays exponentially. The excitation of OTS in the graphene-layer surface leads to a nearly zero-reflectance dip at $\lambda = 315$ μm. Due to this strong field enhancement, the graphene-based OTS can be applied in optical sensors, optical filters, etc.

It is known that the excitation of OTS corresponds to a common solution of the wave equation, which is a superposition of the electromagnetic wave localized at the graphene top-layer interface. In order to further understand the excitation mechanism and condition of OTS at the interface of the air–graphene top layer, we need to derive the OTS dispersion characteristics of the monolayer graphene. By matching the boundary conditions to the graphene–1D-PC composite configuration in Fig. 1, the OTS dispersion can be derived. Figures 4(b) and 4(d) illustrate the OTS dispersion for the monolayer graphene as a function of wavelength in the THz region and the incident angle. Other parameters have the same values as those in Fig. 2. It is found that this dispersion curve is in accord with the results in Figs. 4(a) and 4(c). These results indicate that the OTS can generate for both TE- and TM-polarizations even at normal incidence without the need for prism coupling, and the resonant wavelength is blue shifted with the increasing of the incident angle for both polarizations. Furthermore, it can be clearly seen from Fig. 4 that both the TM polarization state and the TE polarization state are degenerating under normal incidence. They require the same resonance frequency for the excitation of OTS. However, the frequency for exciting TM-polarized OTS is higher than the level of the TE-polarized OTS with the increase of the incident angle. Besides, the difference between the two resonance frequencies would also increase with the incident angle. Note that there is no strict sense of gap between the TM-polarized dispersion curve and the low energy bandgap edge for large incidence angle, so we only draw the dispersion curve less than 50°.

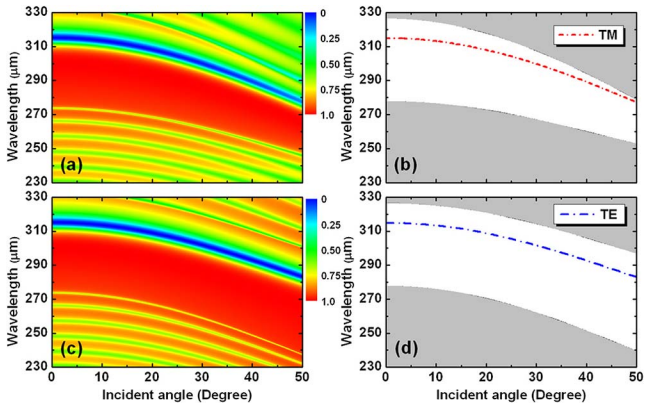

Fig. 4. (a) Dependence of the reflectance for the TM-polarized on wavelength and incident angle. (b) OTS dispersion characteristics on monolayer graphene for the TM-polarized. (c) Dependence of the reflectance for the TE-polarized on wavelength and incident angle. (d) OTS dispersion characteristics on monolayer graphene for the TE-polarized. Other parameters are the same as before.

The theoretical and experimental results show that the resonance energy of OTS in a metal–Bragg-reflector structure can be greatly modulated by the top layer[17,43]. By varying the dispersion parameters of the top layer, one can change the reflection coefficient of the PC as well as the resonance frequency of the OTS. It provides an effective route for tuning the OTS properties of the graphene–1D-PC composite configuration. Here, we only discuss the reflectance dip. Figure 5(a) presents the variation of reflection spectra with wavelengths for different dielectric constants of the top layer. It is found that the reflectance dip could shift to shorter wavelengths by decreasing the dielectric constant of the top layer. However, there is some change in the minimum reflectivity during the PC bandgap range. In addition, the thickness of the top layer has a measurable impact on the reflectance. For the sake of simplicity, we only discuss the case of one OTS, so we only consider the case of thin thickness for the top layer, namely, $d_s \le \lambda/(2n_s)$[2]. It is noteworthy that, for larger d_s, it is possible to excite multiple OTSs in the photonic bandgap. Figure 5(b) also shows the reflection spectra as a function of wavelength for different thicknesses of the top layer. It is clear that the reflectance dip is strongly dependent on the thickness of the top layer. We can obviously find that the reduction of the top layer's thickness d_s could lead to a shift of the OTS to a shorter wavelength. Meanwhile, the minimum value of reflectance would also change slightly. However, the bandwidth of the reflectance dip is widened.

In general, different numbers of layers could easily affect the electrical and optical properties of most 2D materials, including graphene. Therefore, it is necessary to further discuss the impact of graphene's layer number on the excitation of OTS, especially its influence on reflectance

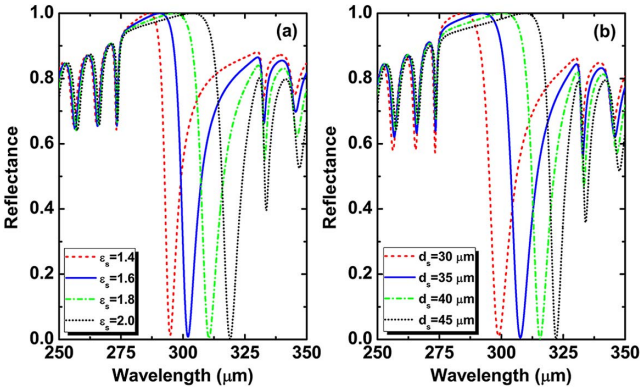

Fig. 5. (a) Reflectance as a function of wavelength at different dielectric constants of the top layer. (b) Reflectance as a function of wavelength at different thicknesses of the top layer. Other parameters have the same values as those in Fig. 2.

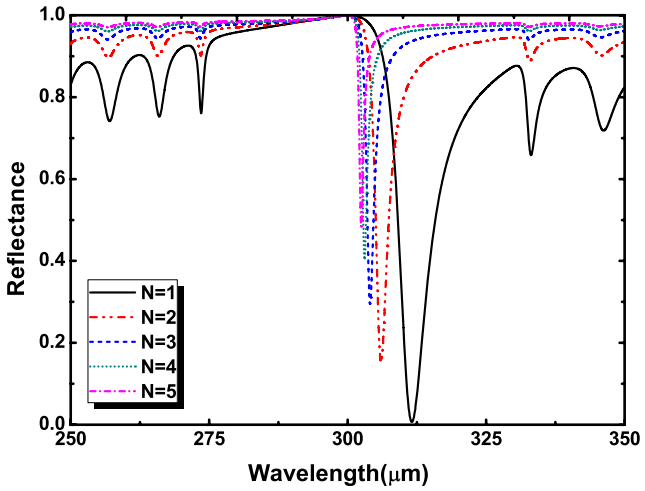

Fig. 6. Reflectance as a function of wavelength at different numbers of layers; here, $E_F = 1.0$ eV. Other parameters have the same values as those in Fig. 2.

dip. As we all know, when the layer number of few-layer graphene satisfies $N < 6$, there would be an approximate linear relationship between its conductivity and the layer number[44]. The influence of graphene's layer number on reflectance dip is illustrated in Fig. 6. It is clear that the whole reflectance dip is shifting toward a shorter wavelength with the increase of graphene layers, accompanied by a sharp decline of full width at half maximum. This phenomenon can be applied to develop various OTS-based photoelectric devices. Although the increase of graphene layers could lead to sharper reflectance dip, the minimal reflectivity would shift upward slightly. Meanwhile, the maximal number of graphene layers is also limited, as the increase of graphene layers might damage some of its electrical and optical properties or, even worse, could make the graphene a bulk medium.

In conclusion, we have presented a graphene–1D-PC composite configuration to realize OTS in the THz frequency region and discussed the controllable properties of this phenomenon. It is found that the wavelength-dependent reflectance dip is strongly dependent on the optical properties of the graphene sheet as well as the dielectric thickness of the top layer, and the reflectance dip of the wavelength can be tuned by changing the Fermi energy applied on the graphene sheets. Moreover, we have discussed the dispersion characteristics on monolayer graphene as a function of wavelength and incident angle. Since the structure can be built with planar fabrication techniques, it offers an interesting approach to tunable OTS. We believe that the controllable OTS phenomenon at the THz frequency could have potential applications in optical filters, optical absorption, and some other optoelectronics fields.

This work was partially supported by the National Natural Science Foundation of China (Nos. 11704119, 61505111, 61575127, and 61490713), the Natural Science Foundation of Hunan Province (No. 2018JJ3325), the Natural Science Foundation of Guangdong Province (No. 2015A030313549), the Science and Technology Planning Project of Guangdong Province (No. 2016B050501005), and the Scientific Research Fund of Hunan Provincial Education Department (No. 17C0945).

References

1. A. V. Kavokin, I. A. Shelykh, and G. Malpuech, Phys. Rev. B **72**, 233102 (2005).
2. M. Kaliteevski, I. Iorsh, S. Brand, R. A. Abram, J. M. Chamberlain, A. V. Kavokin, and I. A. Shelykh, Phys. Rev. B **76**, 165415 (2007).
3. A. Kavokin, I. Shelykh, and G. Malpuech, Appl. Phys. Lett. **87**, 261105 (2005).
4. W. L. Barnes, A. Dereux, and T. W. Ebbesen, Nature **424**, 824 (2003).
5. C. Symonds, G. Lheureux, J. P. Hugonin, J. J. Greffet, J. Laverdant, G. Brucoli, A. Lemaitre, P. Senellart, and J. Bellessa, Nano Lett. **13**, 3179 (2003).
6. B. J. Lee, Y. B. Chen, and Z. M. Zhang, Opt. Lett. **33**, 204 (2008).
7. M. Fang, F. Shi, and Y. Chen, Plasmonics **11**, 197 (2015).
8. S. Brand, M. A. Kaliteevski, and R. A. Abram, Phys. Rev. B **79**, 085416 (2009).
9. T. Goto, A. V. Dorofeenko, A. M. Merzlikin, A. V. Baryshev, A. P. Vinogradov, M. Inoue, A. A. Lisyansky, and A. B. Granovsky, Phys Rev Lett. **101**, 113902 (2008).
10. T. Goto, A. V. Baryshev, M. Inoue, A. V. Dorofeenko, A. M. Merzlikin, A. P. Vinogradov, A. A. Lisyansky, and A. B. Granovsky, Phys. Rev. B **79**, 125103 (2009).
11. A. B. Khanikaev, A. V. Baryshev, M. Inoue, and Y. S. Kivshar, Appl. Phys. Lett. **95**, 011101 (2009).
12. T. Hu, Y. Wang, L. Wu, L. Zhang, Y. Shan, J. Lu, J. Wang, S. Luo, Z. Zhang, L. Liao, S. Wu, X. Shen, and Z. Chen, Appl. Phys. Lett. **110**, 051101 (2017).
13. N. Lundt, S. Klembt, E. Cherotchenko, S. Betzold, O. Iff, A. V. Nalitov, M. Klaas, C. P. Dietrich, A. V. Kavokin, S. Höfling, and C. Schneider, Nat. Commun. **7**, 13328 (2016).
14. J. Guo, Y. Sun, Y. Zhang, H. Li, H. Jiang, and H. Chen, Phys. Rev. E **78**, 026607 (2008).
15. Z. Chen, P. Han, C. W. Leung, Y. Wang, M. Hu, and Y. Chen, Opt. Express **20**, 21618 (2012).
16. O. E. Abouti, E. H. E. Boudouti, Y. E. Hassouani, A. Noual, and B. Djafari-Rouhani, Phys. Plasmas **23**, 082115 (2016).
17. M. E. Sasin, R. P. Seisyan, M. A. Kalitteevski, S. Brand, R. A. Abram, J. M. Chamberlain, A. Y. Egorov, A. P. Vasilev, V. S. Mikhrin, and A. V. Kavokin, Appl. Phys. Lett. **92**, 251112 (2008).
18. H. Zhou, G. Yang, K. Wang, H. Long, and P. Lu, Opt. Lett. **35**, 4112 (2010).
19. Y. Gong, X. Liu, H. Lu, L. Wang, and G. Wang, Opt. Express **19**, 18393 (2011).
20. H. X. Da, Z. Q. Huang, and Z. Y. Li, Opt. Lett. **34**, 1693 (2009).
21. G. Lu, J. Da, Q. Mo, and P. Chen, Phys. B: Condens. Matter **406**, 4159 (2011).
22. B. Guo, Chin. Opt. Lett. **16**, 020004 (2018).
23. H. Zhang, Q. Bao, D. Tang, L. Zhao, and K. Loh, Appl. Phys. Lett. **95**, 141103 (2009).
24. H. Zhang, D. Tang, R. J. Knize, L. Zhao, Q. Bao, and K. P. Loh, Appl. Phys. Lett. **96**, 111112 (2010).
25. Y. Xiang, X. Dai, J. Guo, H. Zhang, S. Wen, and D. Tang, Sci. Rep. **4**, 5483 (2014).
26. S. C. Dhanabalan, J. S. Ponraj, H. Zhang, and Q. Bao, Nanoscale **8**, 6410 (2016).

27. Q. You, Y. Shan, S. Gan, Y. Zhao, X. Dai, and Y. Xiang, Opt. Mater. Express **8**, 3036 (2018).
28. J. Shi, Z. Li, D. K. Sang, Y. Xiang, J. Li, S. Zhang, and H. Zhang, J. Mater. Chem. C **6**, 1291 (2018).
29. J. S. Ponraj, Z.-Q. Xu, S. C. Dhanabalan, H. Mu, Y. Wang, J. Yuan, P. Li, S. Thakur, M. Ashrafi, K. Mccoubrey, Y. Zhang, S. Li, H. Zhang, and Q. Bao, Nanotechnology **27**, 462001 (2016).
30. Q. Bao, H. Zhang, B. Wang, Z. Ni, C. H. Y. X. Lim, Y. Wang, D. Y. Tang, and K. P. Loh, Nat. Photon. **5**, 411 (2011).
31. P. Tang, Y. Tao, Y. Mao, M. Wu, Z. Huang, S. Liang, X. Chen, X. Qi, B. Huang, J. Liu, and C. Zhao, Chin. Opt. Lett. **16**, 020012 (2018).
32. M. A. K. Othman, C. Guclu, and F. Capolino, J. Nanophoton. **7**, 073089 (2013).
33. M. A. K. Othman, C. Guclu, and F. Capolino, Opt. Express **21**, 7614 (2013).
34. Y.-C. Chang, C.-H. Liu, C.-H. Liu, S. Zhang, S. R. Marder, E. E. Narimanov, Z. Zhong, and T. B. Norris, Nat. Commun. **7**, 10568 (2016).
35. T. Gric and O. Hess, Opt. Express **25**, 11466 (2017).
36. D. Sun, M. Wang, Y. Huang, Y. Zhou, M. Qi, M. Jiang, and Z. Ren, Chin. Opt. Lett. **15**, 051603 (2017).
37. F. Bonaccorso, Z. Sun, T. Hasan, and A. C. Ferrari, Nat. Photon. **4**, 611 (2010).
38. G. Lu, K. Yu, Z. Wen, and J. Chen, Nanoscale **5**, 1353 (2013).
39. P. Tassin, T. Koschny, M. Kafesaki, and C. M. Soukoulis, Nat. Photon. **6**, 259 (2012).
40. G. Zheng, M. Qiu, F. Xian, Y. Chen, L. Xu, and J. Wang, Appl. Phys. Express **10**, 092202 (2017).
41. T. Zhan, X. Shi, Y. Dai, X. Liu, and J. Zi, J. Phys. Condens. Matter. **25**, 215301 (2013).
42. A. Podzorov and G. Gallot, Appl. Opt. **47**, 3254 (2008).
43. M. E. Sasin, R. P. Seisyan, M. A. Kaliteevski, S. Brand, R. A. Abram, J. M. Chamberlain, I. V. Iorsh, I. A. Shelykh, A. Y. Egorov, A. P. Vasil'ev, V. S. Mikhrin, and A. V. Kavokin, Superlattices Microstruct. **47**, 44 (2010).
44. C. Casiraghi, A. Hartschuh, E. Lidorikis, H. Qian, H. Harutyunyan, T. Gokus, K. S. Novoselov, and A. C. Ferrari, Nano Lett. **7**, 2711 (2007).